Chandra X-ray Observatory Mirror Effective Area

Ping Zhao, Diab Jerius, Richard J. Edgar, Terrance J. Gaetz, Leon P. Van Speybroeck, Beth Biller, Eli Beckerman

Smithsonian Astrophysical Observatory
60 Garden Street, Cambridge, MA 02138

Herman L. Marshall

Massachusetts Institute of Technology

HRMA Effective Area

The HRMA Effective Area is one of the most important parameters of the Chandra X-ray Observatory. It has been calibrated to an unprecedented precision for any X-ray telescope, to ensure an accurate measurement of the flux from X-ray sources. We discuss the HRMA Effective Area measurements, based on the ground calibration made at the X-Ray Calibration Facility in Marshall Space Flight Center. We present the derivations of both on-axis and off-axis effective areas, which are currently in the CALDB and used by Chandra observers.

Outline

- Calibration of the HRMA HRMA Effective Area.
- SAOsac Raytrace simulation
- Ir Optical constants
- Comparison of data with model
- HRMA effective area predictions
- Summary and unresolved issues.

HRMA Calibration Configuration at XRCF

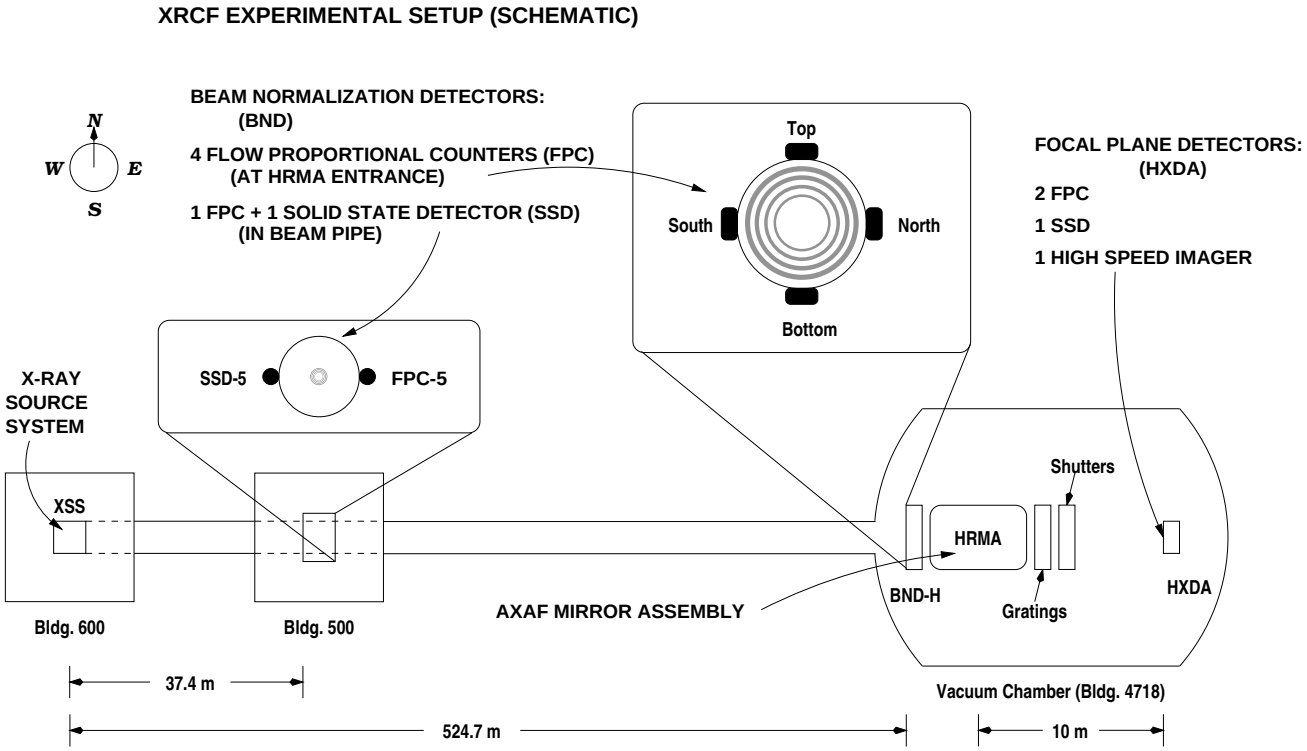

Figure 1: XRCF Calibration configuration

X-ray sources:

- **X-ray line source.**
- **C-continuum source.**
- **W-continuum DCM source**

Detectors:

- **Germanium Solid State Detector (SSD).**
- **Flow Proportional Counter (FPC).**

Shutters:

- **16 Shutters behind the HRMA. One for each quadrant of each shell.**

XRCF measurements for the HRMA Effective Area

- **SSD C-continuum Measurements:**
  - **X-ray source: C-continuum (0.5 – 10 keV)**
  - **Focal plane detector: SSD-X**
  - **Beam normalization detector: SSD-5**
  - **Apertures: 5 mm for SSD-X, 2 mm for SSD-5**
  - **Measurements: individual shells 1, 3, 4, 6**
- **SSD Spectral line Measurements**
  - **X-ray source: Nb-La (2.17 keV), Ag-La (2.98 keV), Sn-La (3.44 keV)**
  - **Focal plane detector: SSD-X**
  - **Beam normalization detector: SSD-5**
  - **Apertures: 5 mm for SSD-X, 2 mm for SSD-5**
  - **Measurements: Full HRMA**
- **FPC Spectral line Measurements**
  - **X-ray source: C-Ka (0.277 keV), Cu-La (0.9297 keV), Al-Ka (1.486 keV), Ti-Ka (4.51 keV), Cr-Ka (5.41 keV), Fe-Ka (6.4 keV), Cu-Ka (8.03 keV)**
  - **Focal plane detector: FPC-X2**
  - **Beam normalization detector: FPC-Hs**
  - **Apertures: 2 mm and 35 mm for FPC-X2, 35 mm for FPC-Hs**
  - **Measurements: individual shells and full HRMA**
- **DCM W-continuum Measurements**
  - **X-ray source: W-continuum DCM source (2 – 10 keV)**
  - **Focal plane detector: FPC-X2**
  - **Beam normalization detector: FPC-Hs**
  - **Apertures: 35 mm for FPC-X2, 35 mm for FPC-Hs**
  - **Measurements: Full HRMA**

C-continuum SSD measurements and data reduction

- **The On-axis Effective Area measurement were made for each shell. Figure 3 shows the SSX and SS5 spectra of these four measurements.**
- **Pileup Corrections were made to correct photo pileups at $E <$ 2keV. Figure 4 show the Pileup Corrections for the four measurements.**
- **Deadtime Corrections were made using the injected pulsers.**
- **Beam Uniformity was measured by scan SSD-5. The Flux Ratio (FR) of SSD-5 home position vs. the optical axis was fit as a function of X-ray energy in E, in unit of keV as:**

$$FR = 1.01341 - 0.00512E + 0.000567E^2 \quad (1)$$

with a relative error of 0.0034.

- **SSD Icing Effect: SSD measurement for $E < 2\ keV$ are not reliable.**
- **Background: $2 - 9 \times 10^{-5}$ c/s/ch, which is negligible in our data analysis.**
- **The relative QE of SS5/SSX was measured, by swapping the two SSDs, to be $R(E) = 1.0141 \pm 0.0089$.**
- **SSD Energy Scale: Using the characteristic X-ray lines atop the continuum spectra for a linear fit:**

$$Energy = a + b \cdot Channel$$

X-ray Line	Energy
Si-Kα, W-Mα and W-Mβ	1.77525 keV
Ca-Kα	3.69048 keV
Ti-Kα	4.50885 keV
V-Kα	4.94968 keV
Fe-Kα	6.39951 keV
W-Lα	8.37680 keV

Figure 5 show the SSX and SS5 energy scales fitted with the six X-ray line energies.

Measured Effective Area

For the C-continuum SSD measurements, the HRMA mirror effective area, $A_{eff}(E)$, is:

$$A_{eff}(E) = \frac{C_{ssx}(E)}{C_{ss5}(E)} \cdot \frac{PDC_{ssx}}{PDC_{ss5}} \cdot \frac{D_{hrma}^2}{D_{ss5}^2} \cdot A_{ss5} \cdot R(E) \qquad (2)$$

where

- $C_{ssx}(E)$ **and** $C_{ss5}(E)$ **are the SSX and SS5 spectra with the correct energy scale and equal energy bins (in units of counts/second/keV).**
- PDC_{ssx} **and** PDC_{ss5} **are the pulser deadtime corrections for the SSX and SS5.**
- $D_{hrma} =$ **526.01236 meter is the distance from the source to the HRMA pre-collimater entrance, where the effective area is defined.**
- $D_{ss5} =$ **38.199 meters is the distance from the source to SS5.**
- A_{ss5} **is the SS5 aperture area. A 2 mm aperture was used for all the measurements. Its actual equivalent diameter is 1.9990** $\pm$ **0.0073 mm. So** $A_{ss5} =$ **0.031385** $\pm$ **0.00023 cm**^{2}
- $R(E) =$ **1.0141** $\pm$ **0.0089 is the relative SS5/SSX quantum efficiency from the flat field test.**

Raytrace Predictions

- **The HRMA effective area can be calculated based on the HRMA model raytrace simulation and appropriate optical constants, independently from the XRCF measurements.**
- **Optical constants:**

  The complex index of refraction of the reflecting medium is defined as: $\tilde{n} \equiv n - ik \equiv 1 - \delta - i\beta$

  The optical constants δ **and** β **of Ir were derived from the synchrotron measurements of the Chandra mirror witness flats at BNL. Figure 6 shows the Ir optical constants. Figure 7 shows the calculated and measured reflectivities with different grazing angles.**

  Ir optical constants used in the raytrace are from Gullikson-95 table for 0.10 - 0.94keV, and from synchrotron measurements for 0.94 – 10keV.
- **The reflectivity were calculated from coatings of 328Å Ir with 97Å Cr undercoating on Zerodur base.**

Comparison of measurements with Raytrace

- As shown in Figure 8, there are some discrepancies between the measurements and the raytrace for individual shells, especially for shell 1. But the agreement is reasonably good for the full HRMA (Figure 9).
- A 4th order polynomial was fit to each of the effective area ratios of SSD-data/raytrace for $E > 2keV$. An average ratio of FPC-data/raytrace was used for $E < 2keV$.
- The raytrace EA was scaled by the above ratios and polynomials.
- The FPC measurements were a few percent lower than the SSD measurements. To give equal weights for both SSD and FPC measurements, the EA was further lowered by half the average difference between SSD and FPC.

HRMA Effective Area

- The final XRCF EA is show in Figure 10. It has an error envelop of $\sim 2\%$. This Figure appears in the "Chandra Proposers' Observatory Guide" (POG), Chapter 4, Figure 4.5.
- Use the polynomial curve in Figure 10, we can calibration the HRMA on orbit effective area by scaling the raytrace on-orbit prediction the same way. The predicted on-orbit on-axis (2π) effective area of the HRMA as well as the HRMA times the ACIS or HRC QE are shown in Figure 11. This figure appears in POG, Chapter 4, Figure 4.2.
- The HRMA effective area decreases as the source off-axis angle increases. So the count rate for the same source depends on its off-axis angle. Figure 12 shows the HRMA on-orbit off-axis effective area as a fraction of the on-axis effective area for selected energies, calculated by raytrace simulation. This Figure appears in POG , Chapter 4, Figure 4.4.

DCM W-continuum measurements

- **EA from DCM measurement as a cross check.**
- **Spectral analysis is simplified due to lack of continuum.**
- **Beam uniformity is a problem, especially near strong W lines (1.7,1.8 keV)**
- **Possibly other fitting artifacts.**
- **Detailed structure of effective area curve probably OK.**
- **Large-scale structure may not be reliable as an absolute EA measurement.**
- **Results are comparable to SSD continuum and FPC line results.**
- **The Ir edge structure in the 2-3 keV range is resolved.**
- **Jump near 3 keV is almost certainly the Ar edge in the FPC response.**

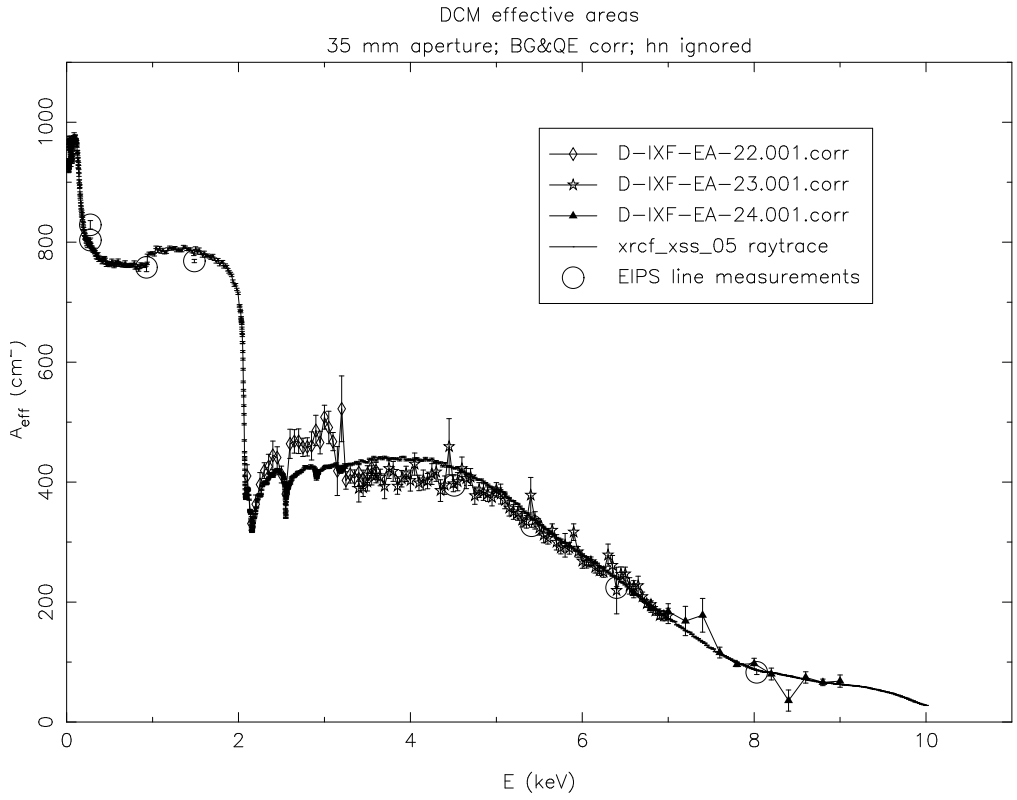

Figure 2: DCM Effective Area Measurements.

Summary

- **The HRMA Effective Area is one of the most important parameters of the Chandra X-ray Observatory.**
- **The HRMA Effective Area has been calibrated to an unprecedented precision for any X-ray telescope, to ensure an accurate measurement of the flux from X-ray sources.**
- **Issues still to be resolved:**
  - **Small discrepancies between SSD and FPC measurements.**
  - **Large discrepancies between measurements and raytrace simulation for shell 1.**
  - **Possible discontinuity at Ir edge ($\sim 2keV$) observed with HETG, which could be due to the mirror surface contamination (see Figure 13).**

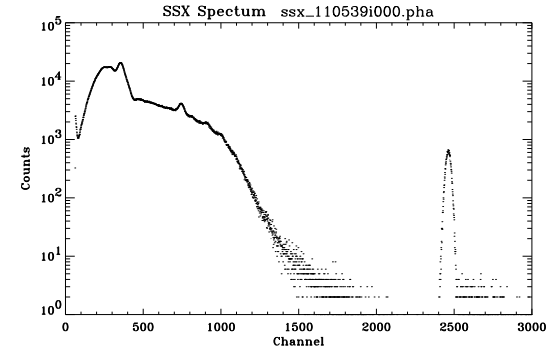

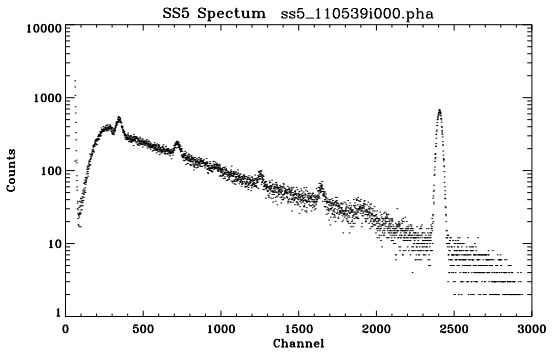

SSX and SS5 spectra: Shell 1.

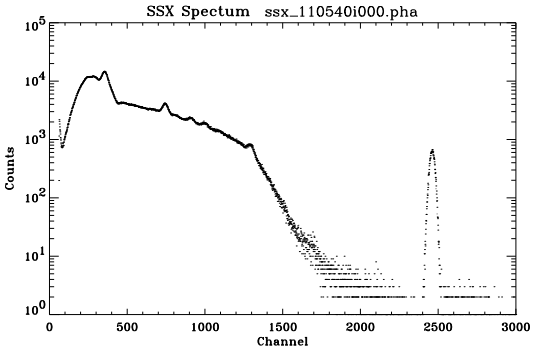

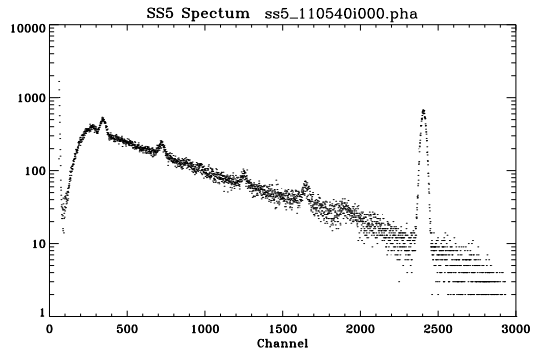

SSX and SS5 spectra: Shell 3.

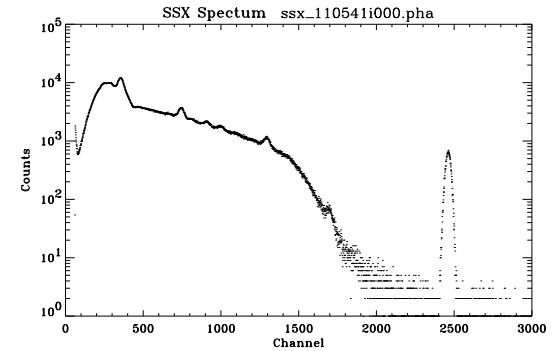

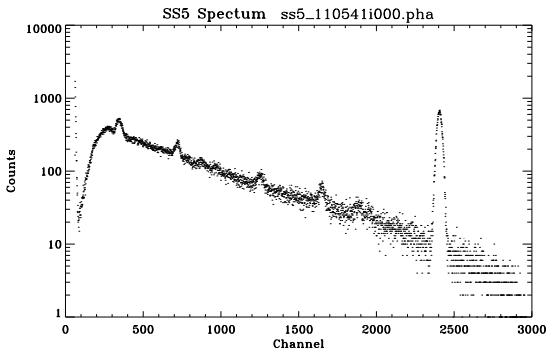

SSX and SS5 spectra: Shell 4.

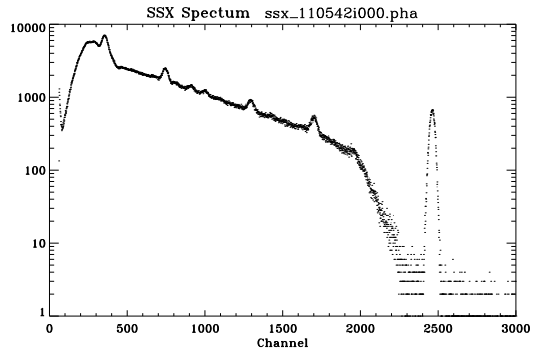

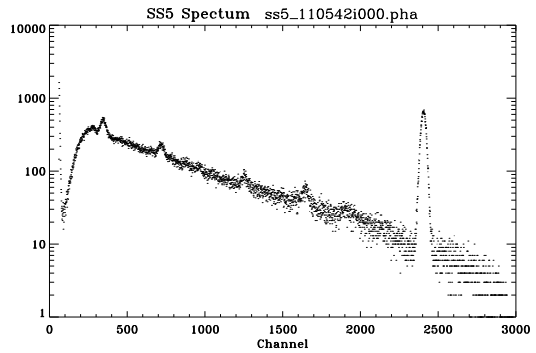

SSX and SS5 spectra: Shell 6.

Figure 3: C-continuum SSX and SS5 spectra of four HRMA shells. Aperture: 2 mm; Integration time: 1000 seconds. The profiles show the C-continuum spectra with several spectral peaks on top. The largest Gaussian-like peak at around channels 2400–2500 is the injected pulser spectrum to be used for the pileup and deadtime corrections. Other peaks are characteristic X-ray lines due to contaminations to the carbon anode. These peaks are used to determine the energy scale.

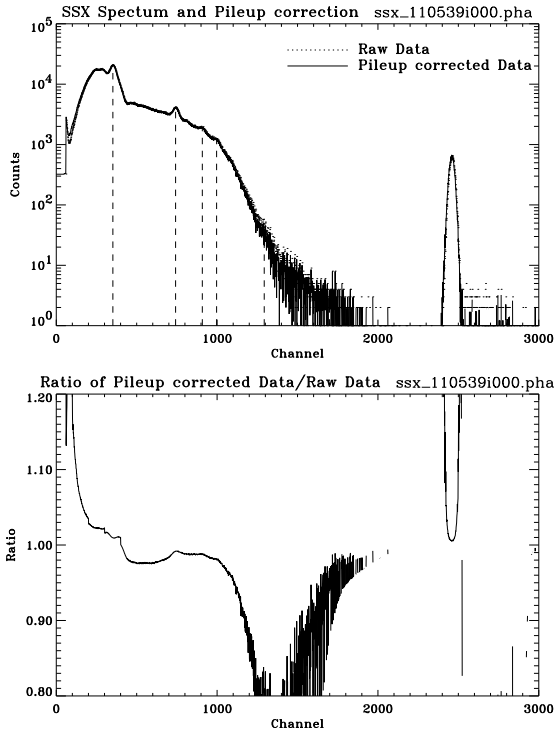

SSX pileup correction: Shell 1; Run ID 110539.

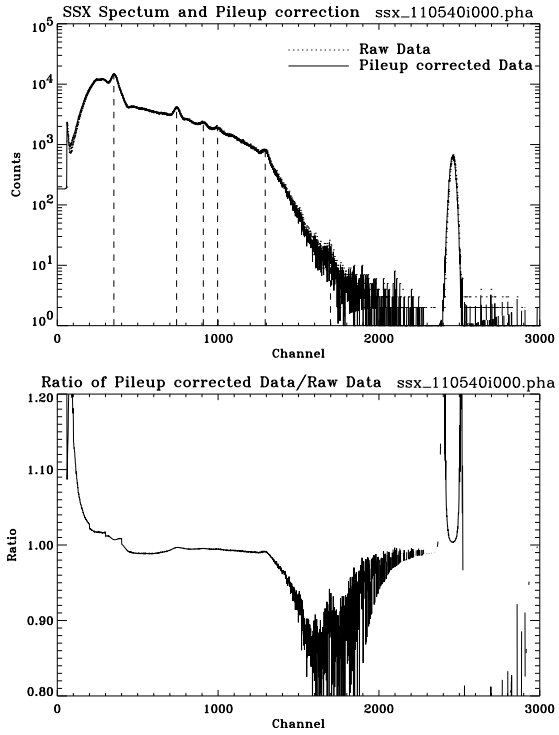

SSX pileup correction: Shell 3; Run ID 110540.

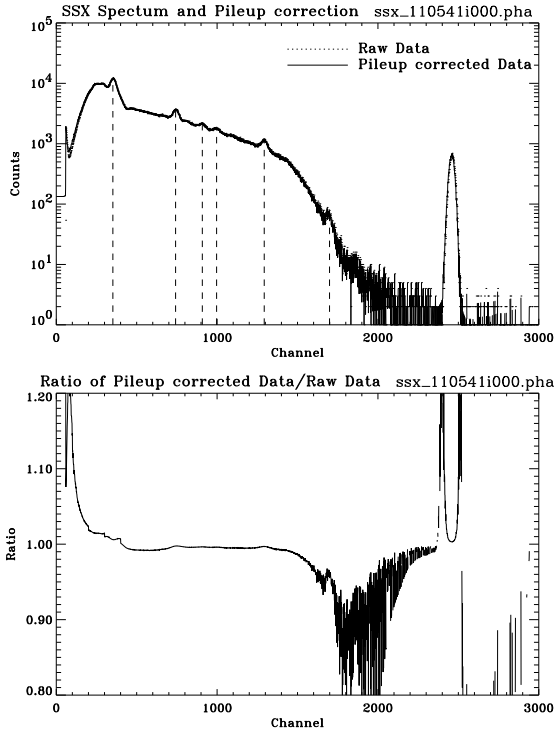

SSX pileup correction: Shell 4; Run ID 110541.

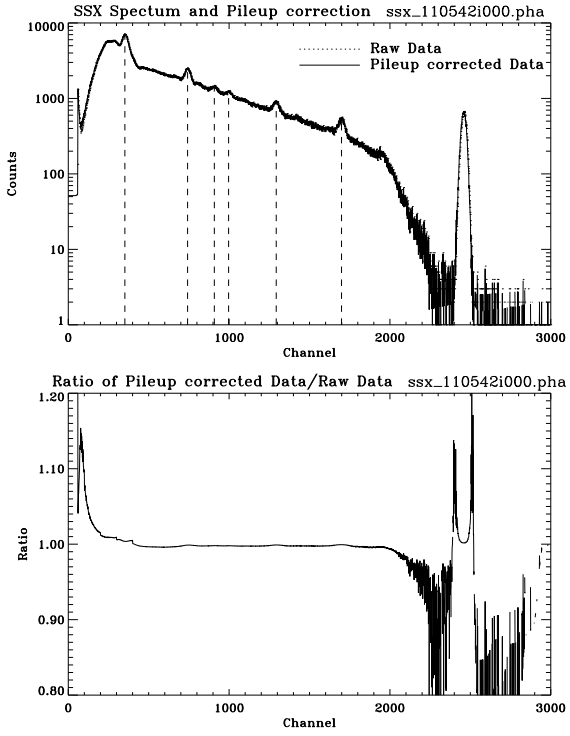

SSX pileup correction: Shell 6; Run ID 110542.

Figure 4: SSX spectra and pileup correction of four shells. Upper panel of each quadrant plot show the raw data and pileup corrected data. Lower panel shows the ratio of pileup corrected data to the raw data.

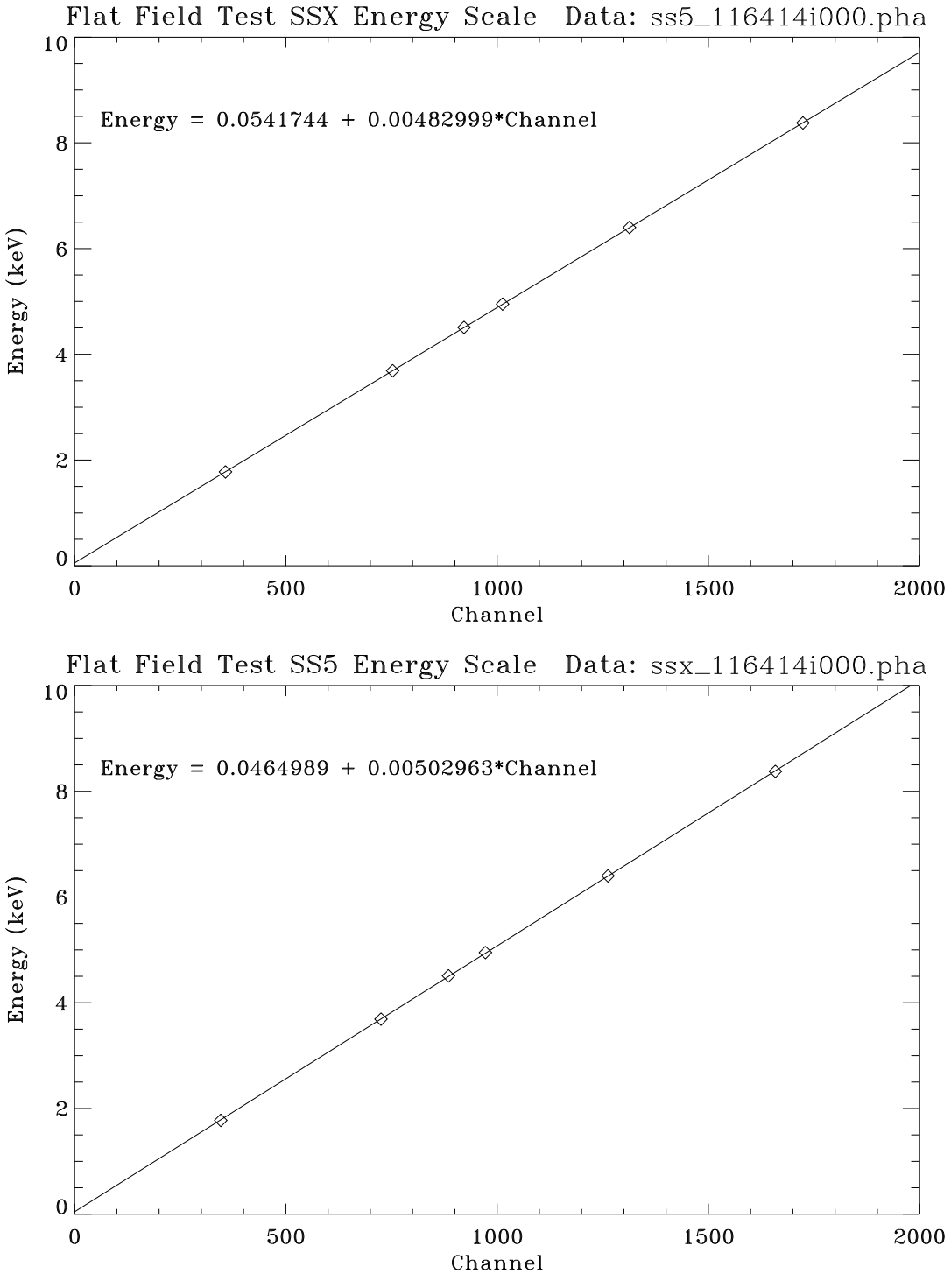

Figure 5: SSX and SS5 energy scales for the flat field test, fitted with six X-ray line energies.

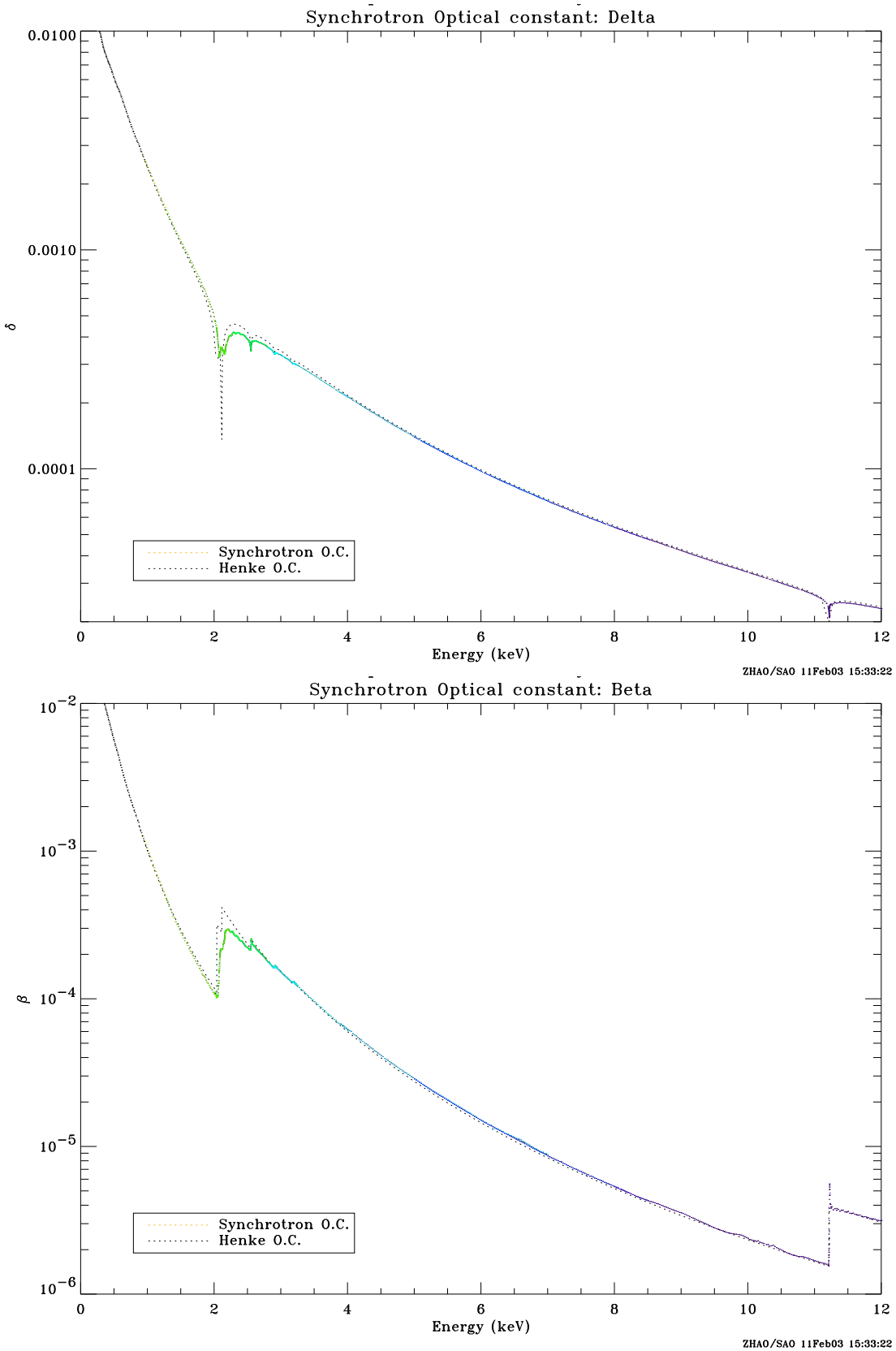

Figure 6: Ir optical constants from the BNL synchrotron measurements.

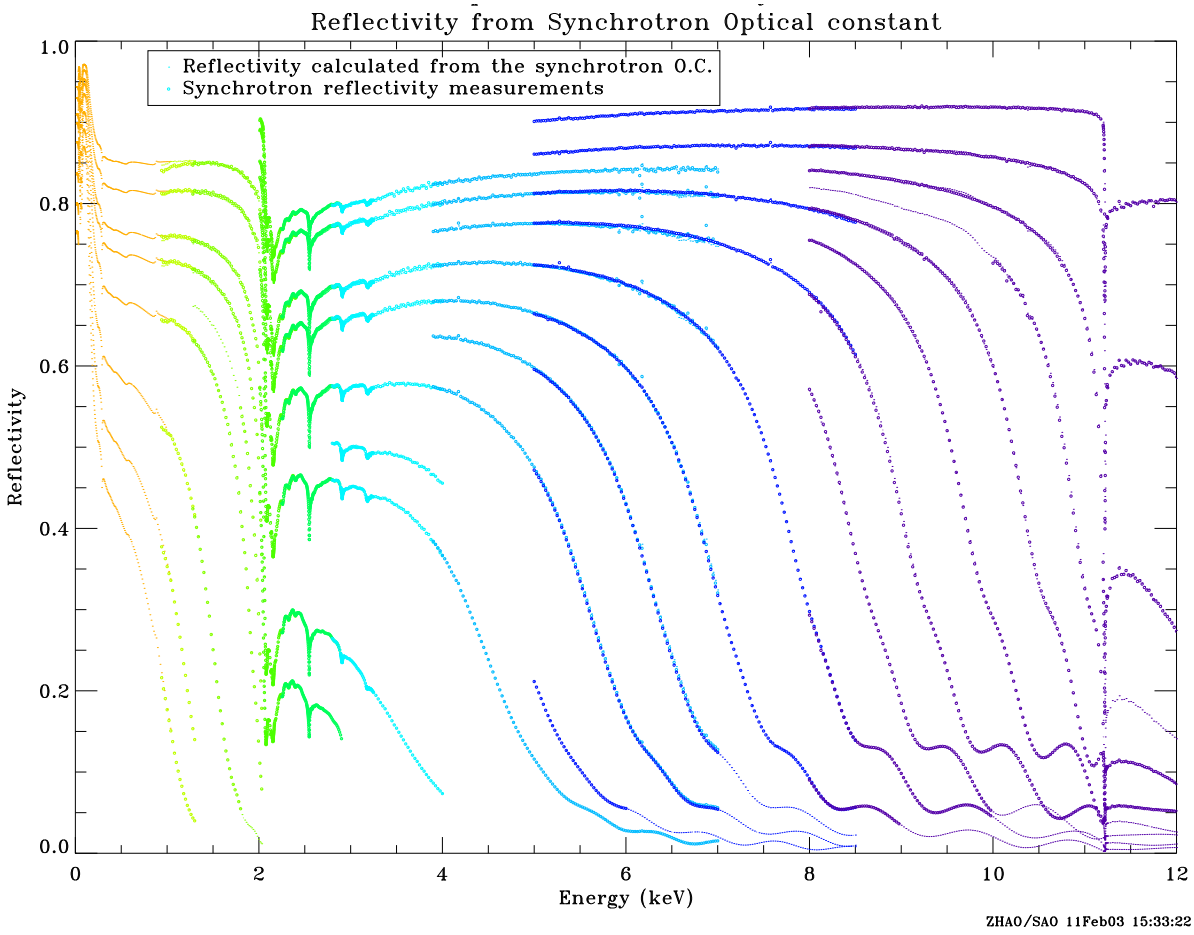

Figure 7: Reflectivity from the Sychrotron Ir optical constants.

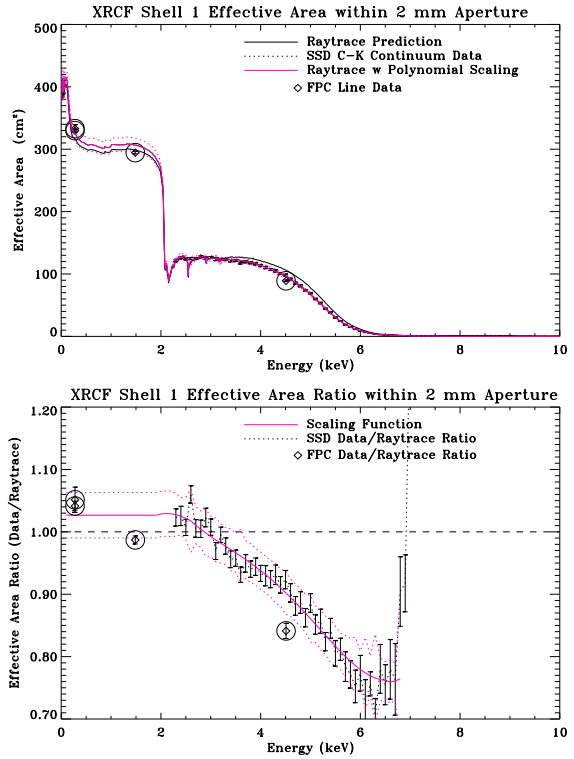

Shell 1.

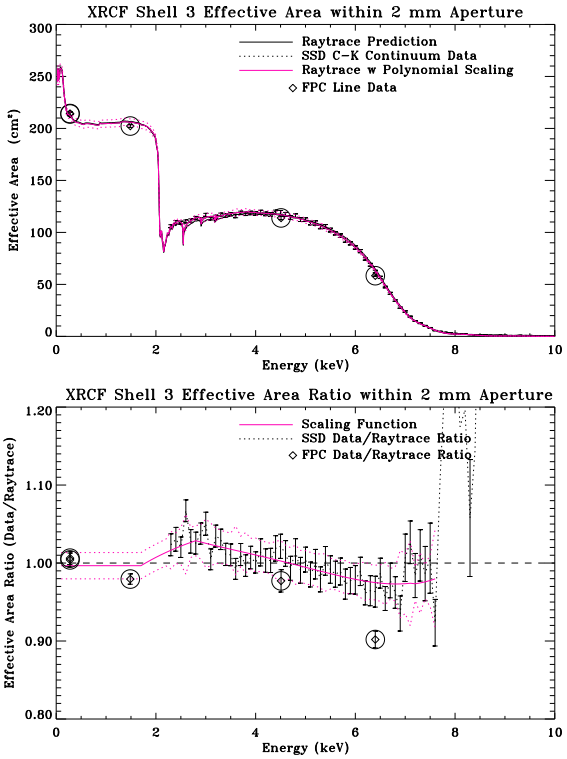

Shell 3.

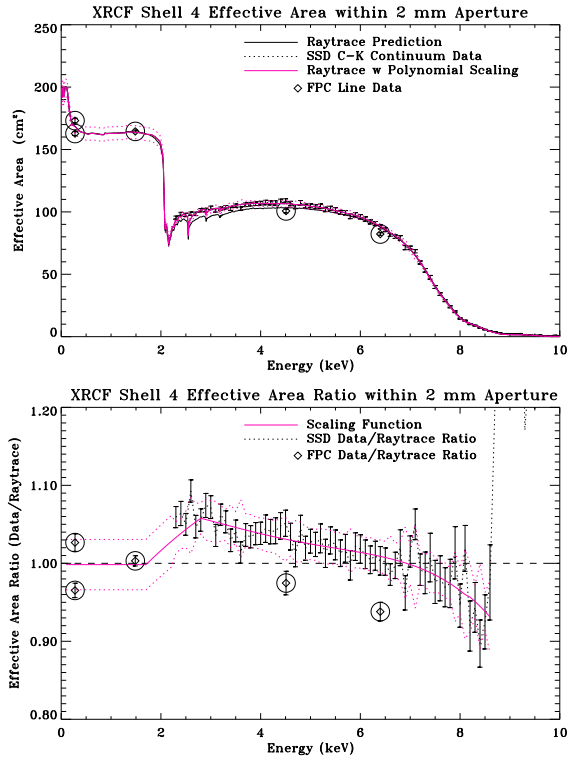

Shell 4.

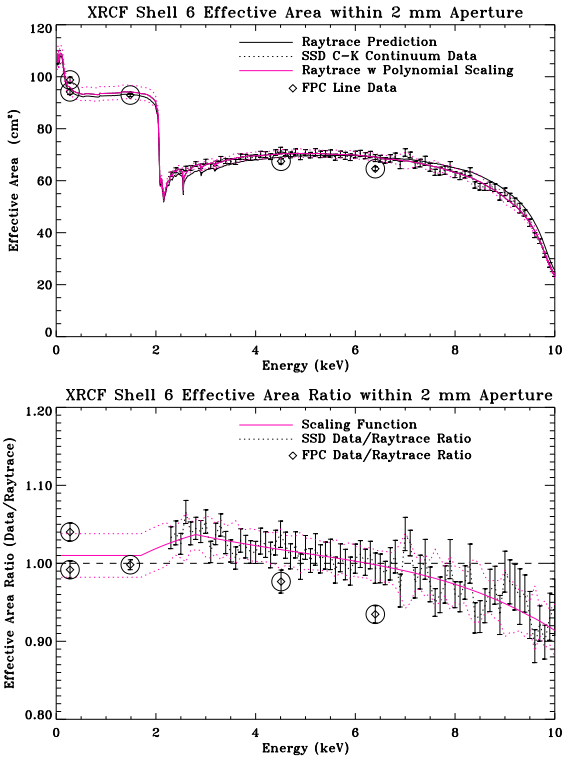

Shell 6.

Figure 8: Calibration data vs. raytrace prediction. Top panel of each quadrant plot shows the XRCF effective area within 2 mm aperture. Bottom panel shows the effective area ratio of data/raytrace.

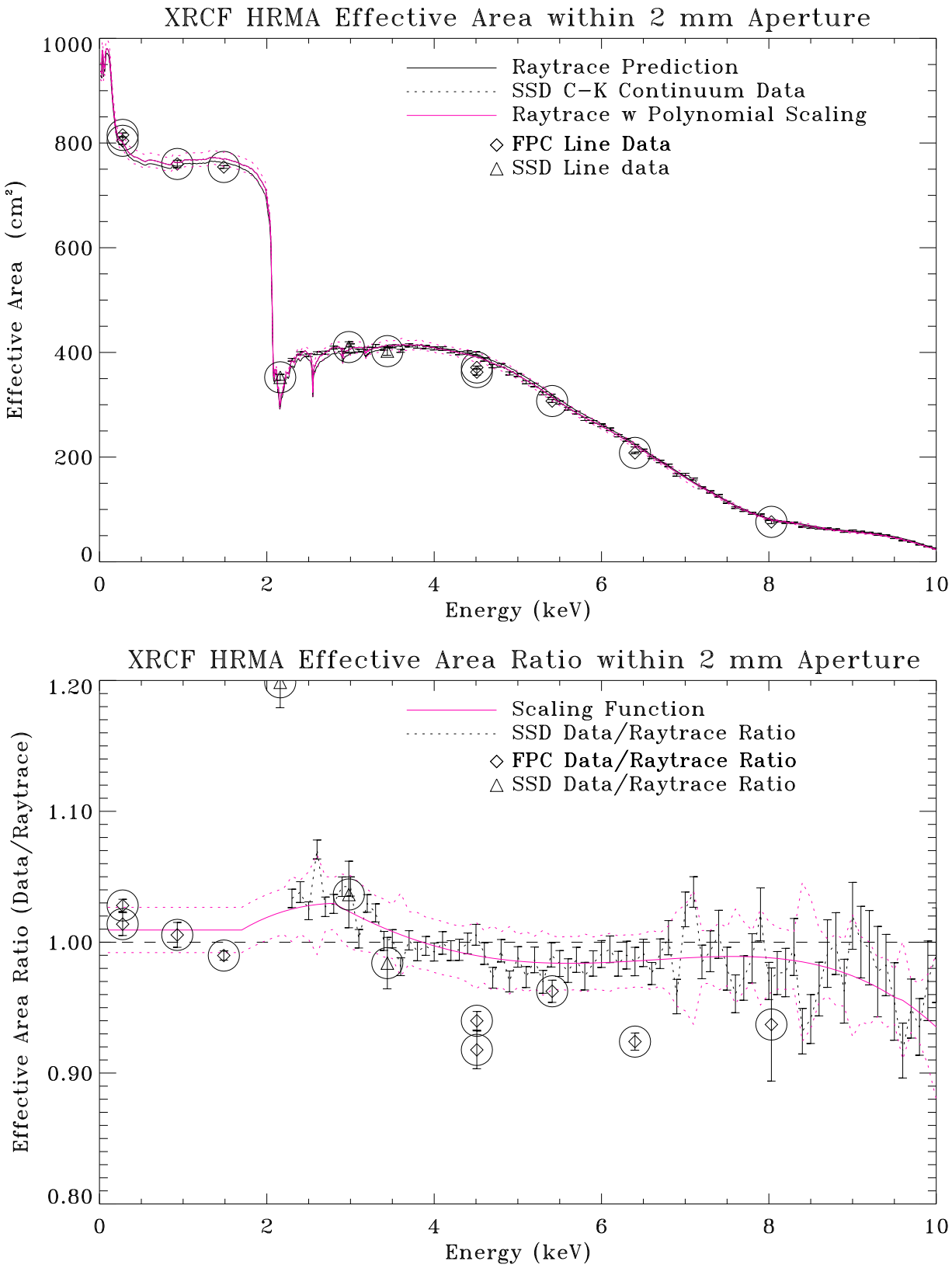

Figure 9: Calibration data vs. raytrace prediction. Top panel shows the XRCF HRMA effective area within 2 mm aperture. Bottom panel shows the effective area ratio of data/raytrace.

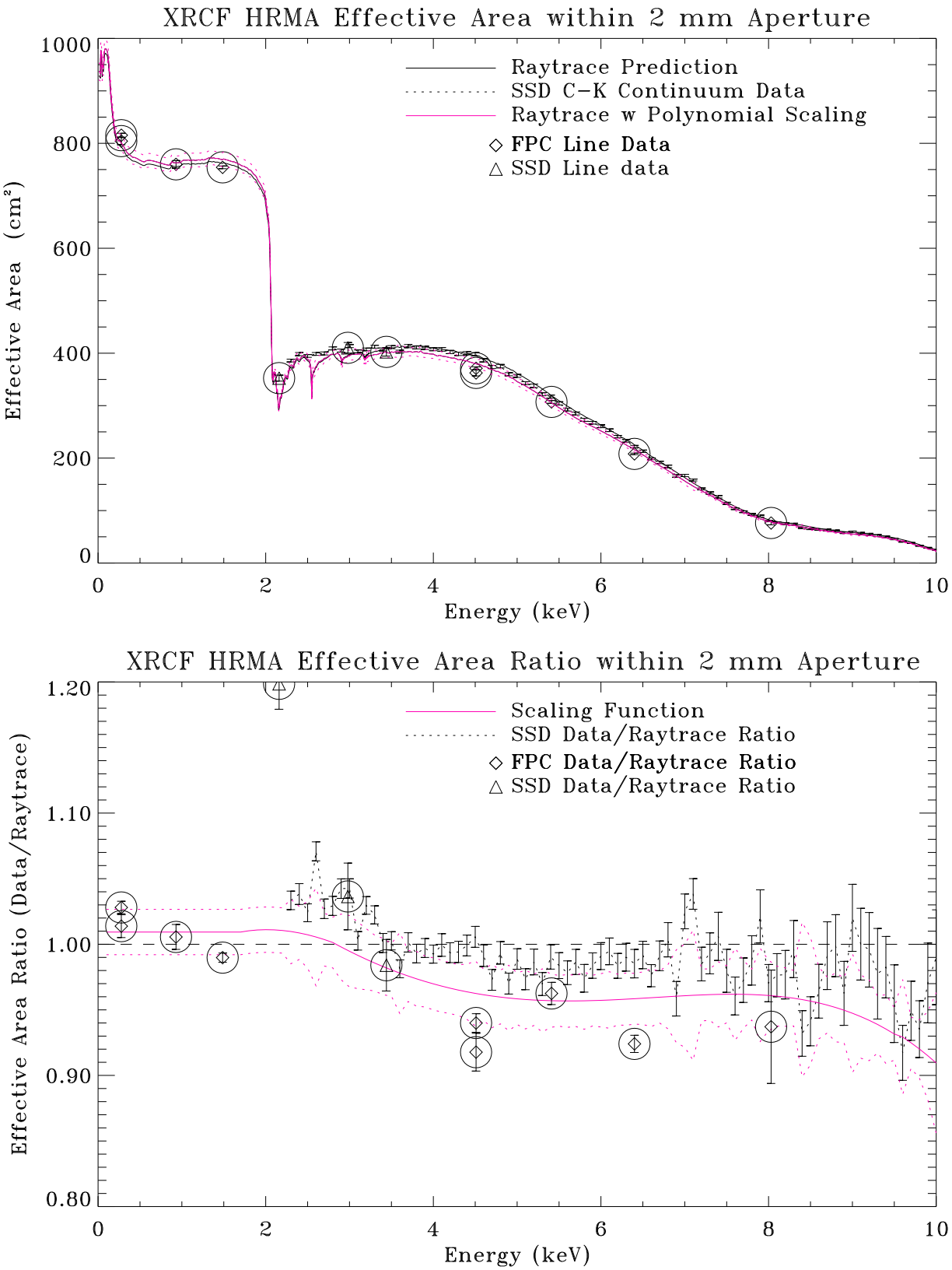

Figure 10: Calibration data vs. raytrace prediction. Top panel shows the XRCF HRMA effective area within 2 mm aperture. Bottom panel shows the effective area ratio of data/raytrace and pulled down by giving 50% the weight to the FPC data.

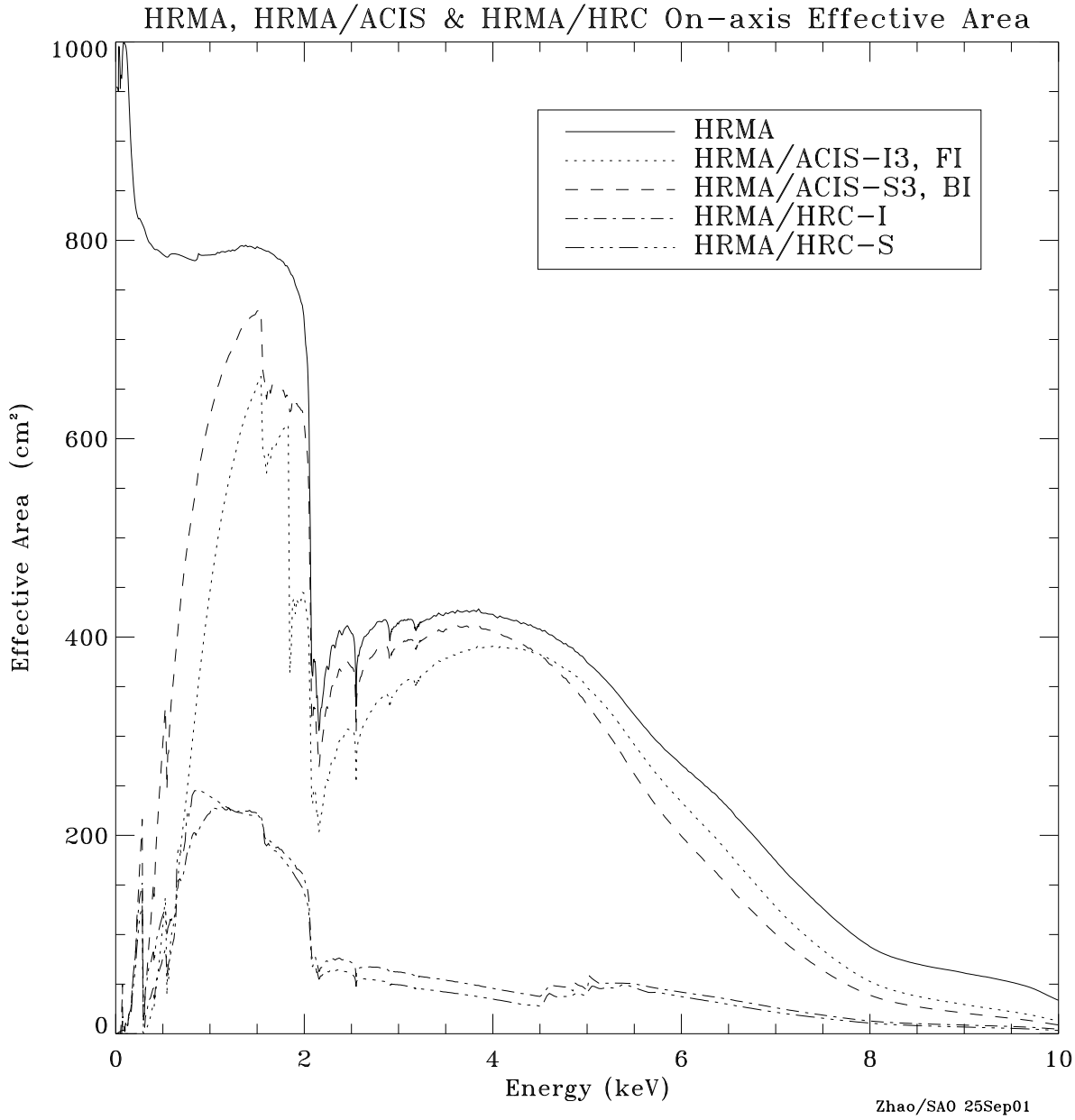

Figure 11: The HRMA, HRMA/ACIS and HRMA/HRC effective areas versus X-ray energy in linear scale. The structure near 2 keV is due to the iridium M-edge. The HRMA effective area is calculated by the raytrace simulation based on the HRMA model and scaled by the XRCF calibration data. The HRMA/ACIS effective areas are the products of HRMA effective area and the Quantum Efficiency (QE) of ACIS-I3 (front illuminated) or ACIS-S3 (back illuminated). The HRMA/HRC effective areas are the products of HRMA effective area and the QE of HRC-I or HRC-S at their aimpoints, including the effect of UV/Ion Shields (UVIS).

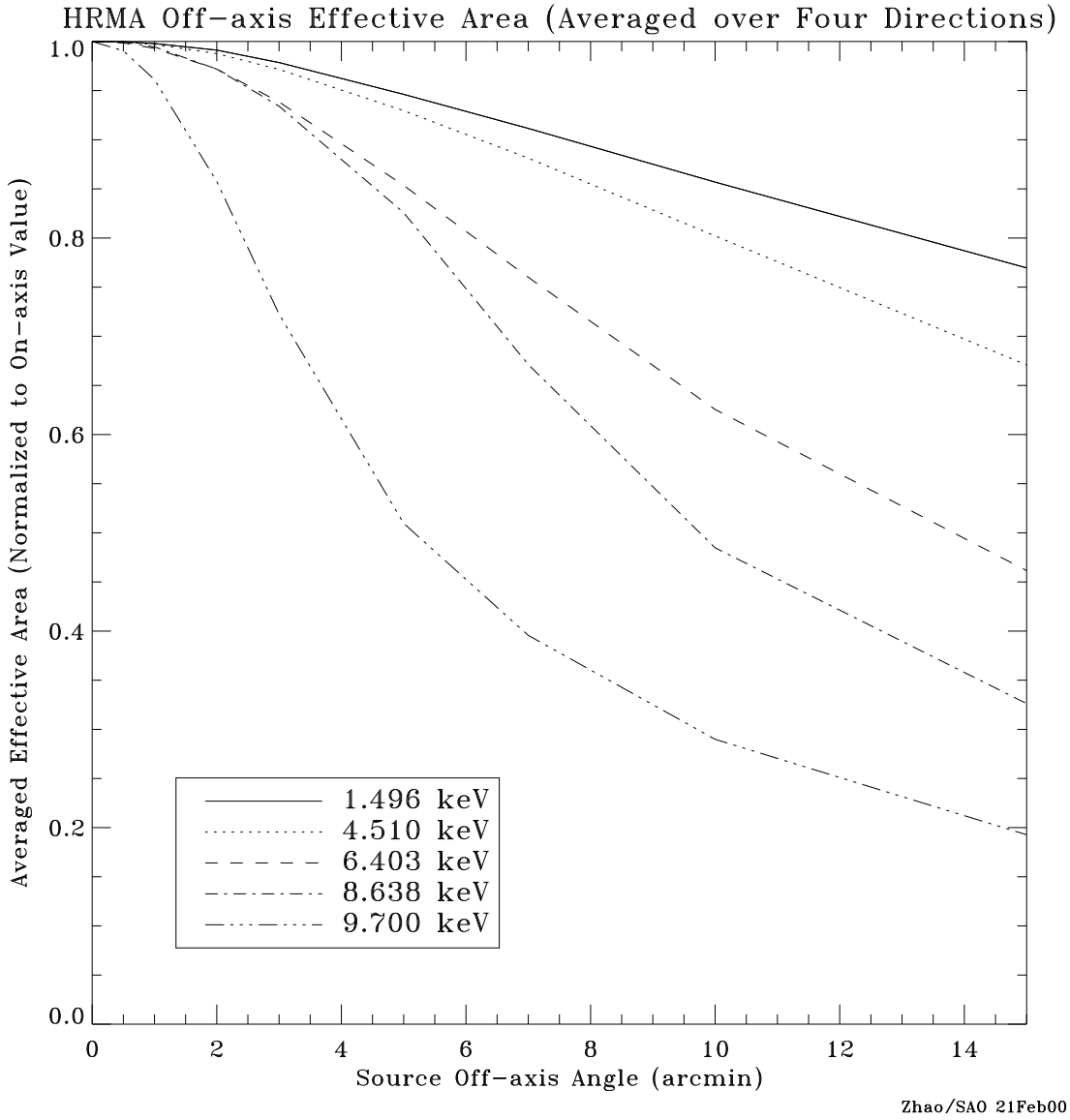

Figure 12: The HRMA effective area versus off-axis angle, averaged over azimuth, for selected energies, normalized to the on-axis area for that energy.

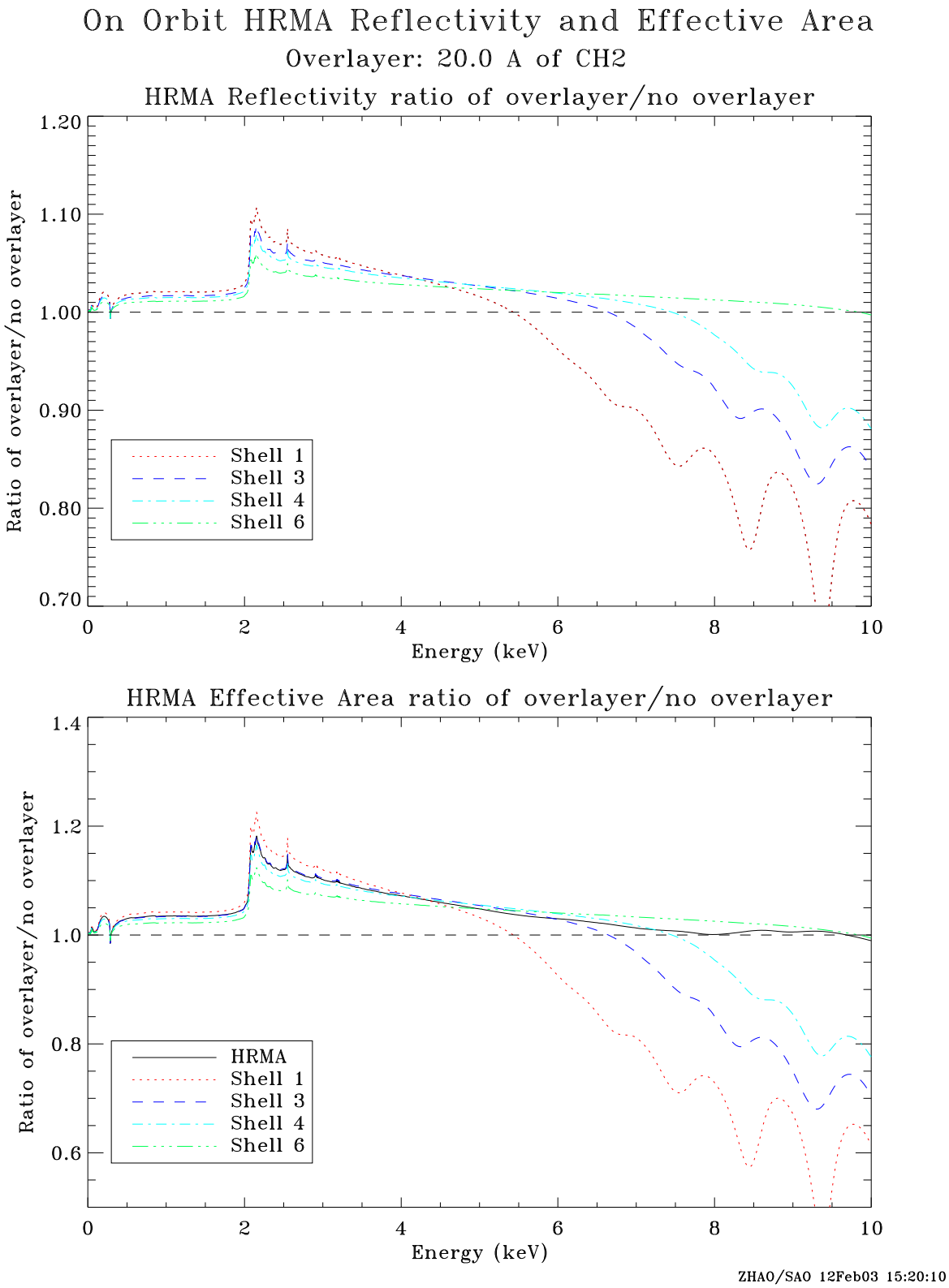

Figure 13: The reflectivity and effective area ratio of the HRMA with and without CH2 overlayers.